Available online at www.sciencedirect.com
SCIENCE DIRECT®
Journal of Sound and Vibration 273 (2004) 233–248
JOURNAL OF SOUND AND VIBRATION
www.elsevier.com/locate/jsvi

On the design of a tunnel-entrance hood with multiple windows

M.S. Howe*

College of Engineering, Boston University, 110 Cummington Street, Boston, MA 02215, USA

Received 23 July 2002; accepted 13 April 2003

Abstract

An analysis is made to determine the optimal distribution of 'windows' in the wall of a long tunnel-entrance hood used to suppress the micro-pressure wave produced when the compression wave generated by an entering high-speed train reaches the far end of the tunnel. An ideally designed hood causes the pressure to rise linearly across a compression wavefront of thickness equal approximately to the ratio of the hood length to the train Mach number. At moderate train Mach numbers the hood length can be assumed to be 'acoustically compact', and the initial form of the compression wave can then be expressed in terms of an equivalent source distribution representing the train and the compact Green's function for sources in the hood. The requirement that the wavefront profile be linear imposes certain conditions on the Green's function that permits the determination of the hood window dimensions. Our calculations take no account of the influence on compression wave formation of separated air flow over the train, from the hood portal and from the peripheries of the windows. The explicit predictions of the optimum window sizes given in this paper may therefore be too small, and should be refined by using model scale tests that allow window dimensions to be varied from their predicted optimal values to incorporate the effects of flow separation.

1. Introduction

The compression wave generated when a train enters a tunnel propagates into the tunnel at the speed of sound, ahead of the train. The pressure rise Δp across the wavefront is equal to a fraction

$$\sim \frac{\gamma M^2}{(1-M^2)}\frac{\mathscr{A}_0}{\mathscr{A}}\left(1+\frac{\mathscr{A}_0}{\mathscr{A}}\right)$$

of the atmospheric pressure p_0, where γ (~ 1.4) is the ratio of specific heats of air, M is the train Mach number, and $\mathscr{A}_0/\mathscr{A}$ is the 'blockage', $\mathscr{A}_0$, $\mathscr{A}$ being, respectively, the cross-sectional areas

*Tel.: +1-617-484-0656; fax: +1-617-353-5866.
E-mail address: mshowe@bu.edu (M.S. Howe).

0022-460X/03/$ - see front matter
doi:10.1016/S0022-460X(03)00498-X

of the train and tunnel [1–6]. Δp can be as large as 2% or 3% of p_0 when the train speed U exceeds about 250 kph, and for a uniform tunnel of equivalent semi-circular radius R the pressure rise occurs across a wavefront of thickness $\sim R/M$.

The acoustic pulse radiated from the distant tunnel exit when the compression wave arrives is called the *micro-pressure wave*. The amplitude of this wave is proportional to the steepness of the compression wavefront when it reaches the exit. Acoustic non-linearity in a long tunnel tends to reduce the wavefront thickness, causing a significant increase in wave steepness, particularly in modern tunnels with 'maintenance-free' (and acoustically 'smooth') concrete slab tracks. The amplitude of the micro-pressure wave can then be large enough to produce vibrations and 'rattles' in buildings near the tunnel exit.

The most common micro-pressure wave countermeasure is the tunnel entrance 'hood'. This consists of a thin-walled extension ahead of the tunnel entrance, whose purpose is to greatly increase the initial 'rise time' of the compression wave: this is achieved by permitting the high-pressure air in front of an entering train to escape through 'windows' distributed along the hood walls [6–8]. The effect of the increased wavefront thickness is to inhibit non-linear steepening and greatly reduce the amplitude of the micro-pressure wave. The compression wavefront generated when a train enters an optimally designed hood of length ℓ_h will have an initial thickness $\sim \ell_h/M$ across which the pressure will rise *linearly* with distance. The window size and spacing for hoods currently in use for conventional high-speed trains ($M \leqslant 0.25$) are determined from model scale tests. This is feasible largely because the hoods are relatively short (typically $\ell_h \sim 3R$) and the time required for a trial and error investigation is not excessive. But $M \sim 0.4$ for newer 'Maglev' trains, and effective suppression of the micro-pressure wave will then require the hood to have a greatly increased length, $\ell_h \sim 10R$ [9]. In these circumstances an ad hoc experimental determination of the optimal window spacing and sizes becomes impracticable.

In this paper an approximate theory is developed for predicting the optimal characteristics of a long hood. Under optimal conditions the initial compression wave thickness $\sim \ell_h/M$ is over twice the hood length ℓ_h, and our theory is therefore based on the assumption that ℓ_h can be regarded as acoustically *compact*. This is strictly a low Mach number approximation, but it is known to yield excellent predictions for a flared hood (with no windows) with $\ell_h = 10R$ for $M = 0.25$ [10]. It is derived by extension of the procedure described in Refs. [10,11], which requires a preliminary calculation of the *compact* Green's function [12] describing the pressure wave radiated into the tunnel from a point source in the vicinity of the hood. The method is a simplified version of the continuum approximation to the distribution of the windows discussed by the author in Refs. [13,14]. On this basis we shall be able to make an approximate prediction of the optimum window sizes when the distribution of window centroids along the hood is prescribed. The prediction will be approximate because vortex 'sources' in the air flow from the windows produced by the passing train are ignored. Those windows far from the hood entrance are relatively small, and are likely to be strongly influenced by separation at the edges, which tends to reduce the effective window 'open area'. Thus, we can expect that our predictions will provide a close approximation to the optimal window dimensions, but that it will be necessary to refine these values by performing experiments that permit small adjustments to the predicted window sizes.

The general formulae describing compression wave formation are reviewed in Section 2; the compact Green's function is discussed in Section 3 for a circular cylindrical hood with an arbitrary prescribed distribution of windows. Typical predictions are discussed in Section 4. Explicit

formulae are presented for a tunnel and hood of the same circular cylindrical cross-section, of the type used in model scale experimental studies [3,5–7,10], but the method is easily modified to deal with more general geometries.

2. Compression wave generated in a compact hood

Consider a circular cylindrical tunnel of radius R and cross-sectional area $\mathscr{A} = \pi R^2$ fitted with a cylindrical hood of the same cross-section having N windows distributed along the hood parallel to the tunnel axis (Fig. 1). Take co-ordinate axes $\mathbf{x} = (x, y, z)$ with the origin O on the cylinder axis in the entrance plane of the hood, with the x-axis coaxial with the cylinder and directed out of the tunnel. To fix ideas let the centroid of the nth window be at $x = x_n,\ y = 0,\ z = R\ (1 \leqslant n \leqslant N)$, $-\ell_h = x_N < x_{N-1} < \cdots < x_1 < 0$, where ℓ_h will be referred to as the length of the hood. The window at x_n may be regarded as curvilinear rectangular with length ℓ_x parallel to the cylinder axis and azimuthal length ℓ_θ.

In the simplest such experimental arrangement, an axisymmetric 'train' of maximum radius h is projected at high speed into the tunnel from $x > 0$, guided by a steel wire tightly stretched along the tunnel axis and threaded through a smooth cylindrical channel bored along the axis of the train. Our discussion will be confined to this case, but our formulae will be applicable also to cases where the train axis is displaced from the tunnel axis. The compression wave is generated as the front of the train passes through the hood. To calculate the initial wavefront profile it may be assumed that the tunnel extends to $x = -\infty$, and that the overall length of the train is very much larger than the 'nose length' L shown in the figure, beyond which the circular cross-sectional area of the train assumes the constant value $\mathscr{A}_0 = \pi h^2$.

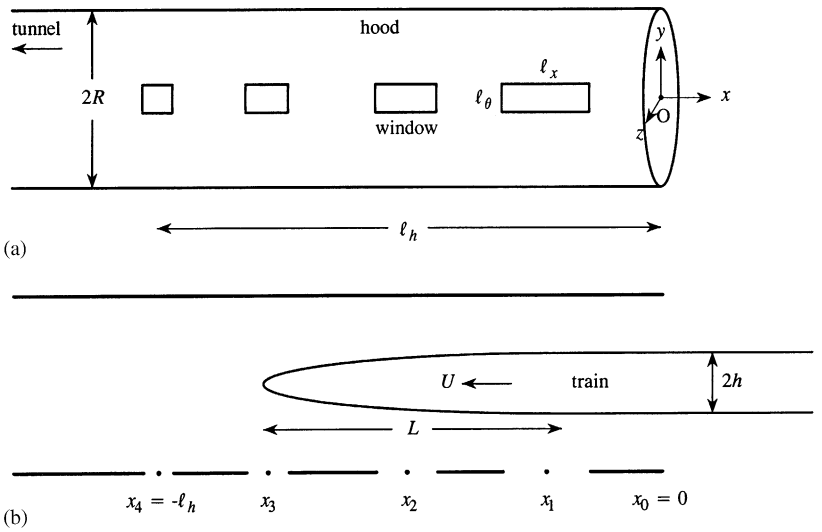

Fig. 1. (a) Schematic of the circular cylindrical tunnel of radius R fitted with a hood of length ℓ_h when there are $N = 4$ rectangular windows. The geometric centre of the nth window is at $x = x_n,\ y = 0,\ z = R$. (b) Characteristic dimensions of an axisymmetric train entering the hood at speed U along the centreline of the tunnel.

The initial pressure rise across the compression wavefront depends on train Mach number and the tunnel blockage. The moving train can be replaced by a uniformly convecting set of monopole and dipole sources that represent the displacement of air by the train and the pressure drag over the nose. The progressive interaction of these distributed sources with the hood portal and windows determine the details of the wavefront profile [5–8,11,12]. Measurements show that, to the rear of the wavefront, the pressure continues to rise slowly with distance from the wavefront. This is usually attributed to aerodynamic sources, i.e., to vorticity in the boundary layers on the train and tunnel walls and in the exit flows from the portal and windows, whose influence on the initial wavefront profile is of secondary importance, and may therefore be ignored in the present discussion.

It is shown in Ref. [11], that when the train enters the tunnel from $x > 0$ along the tunnel-axis at constant speed U, and the blockage $\mathscr{A}_0/\mathscr{A} \leqslant 0.2$ (the case in most applications), the aerodynamic monopole and dipole distributions on the train can be replaced by the following 'slender body approximation'

$$\frac{U}{(1-M^2)}\left(1+\frac{\mathscr{A}_0}{\mathscr{A}}\right)\frac{\partial}{\partial t}\left(\frac{\partial \mathscr{A}_T}{\partial x}(x+Ut)\delta(y)\delta(z)\right), \tag{1}$$

where $\mathscr{A}_T(s)$ denotes the cross-sectional area of the train at distance *s from the front of the nose*, which is assumed to cross the entrance plane ($x = 0$) of the hood at time $t = 0$. The monopole and dipole sources are therefore non-zero only in the vicinity of the train nose where the train cross-section is changing. A corresponding source distribution at the tail of a long train can be ignored when calculating compression wave formation.

The linear acoustic pressure field generated in the tunnel by this source represents the compression wave produced by the train prior to the onset of non-linear steepening. The wavefront properties are determined by the interaction of the nearfield of the moving source with the hood portal and windows as the front of the train travels the length ℓ_h of the hood. The hood is *acoustically compact* when the wavefront thickness is much greater than ℓ_h. Then the compression wave propagates one dimensionally at the speed of sound c_0, say, with pressure $p = p(x,t)$, which is calculated by convolution of source (1) with the compact Green's function for the hood. When the observation point $\mathbf{x}$ lies within the tunnel ahead of the train the Green's function is given by [10–12]

$$G(\mathbf{x},\mathbf{x}';t-\tau) \approx \frac{c_0}{2\mathscr{A}}\left\{\mathrm{H}\left(t-\tau-\frac{|\varphi^*(\mathbf{x})-\varphi^*(\mathbf{x}')|}{c_0}\right)-\mathrm{H}\left(t-\tau+\frac{\varphi^*(\mathbf{x})+\varphi^*(\mathbf{x}')}{c_0}\right)\right\}, \tag{2}$$

where H is the unit step function, and $\varphi^*(\mathbf{x})$ is the velocity potential of a hypothetical incompressible flow *out* of the tunnel portal (from $x = -\infty$); $\varphi^*(\mathbf{x}) \sim O(\sqrt{\mathscr{A}})$ in the vicinity of the portal, and is normalized such that

$$\begin{aligned}\varphi^*(\mathbf{x}) &\approx x-\ell' \quad \text{as } x\to-\infty \text{ inside the tunnel}\\ &\approx -\mathscr{A}/4\pi|\mathbf{x}| \quad \text{as } |\mathbf{x}|\to\infty \text{ outside the tunnel.}\end{aligned} \tag{3}$$

This approximation is applicable for any tunnel whose interior cross-sectional area is ultimately constant and equal to $\mathscr{A}$. The length ℓ' is an 'end-correction' [12,15] whose value depends on the shape of the hood portal and the distribution of the windows. The function $\varphi^*(\mathbf{x})$ satisfies

Laplace's equation $\nabla^2\varphi^* = 0$ and represents an ideal flow from the tunnel that has vanishing circulation about all irreducible closed contours (such as one threading two windows).

The convolution supplies the following formula for the compression wave pressure:

$$p \approx \frac{\rho_0 U^2}{\mathscr{A}(1-M^2)}\left(1+\frac{\mathscr{A}_0}{\mathscr{A}}\right)\int_{-\infty}^{\infty}\frac{\partial \mathscr{A}_T}{\partial x'}(x'+U[t])\frac{\partial \varphi^*}{\partial x'}(x',0,0)\,\mathrm{d}x', \quad \frac{x}{\ell_h}\to-\infty, \tag{4}$$

where ρ_0 is the mean air density and $[t] = t + (x-\ell')/c_0$ is the effective retarded time.

When the potential function $\varphi^*(\mathbf{x})$ is determined numerically it is actually more convenient to calculate first the compression wave 'pressure gradient' $\partial p/\partial t$. By differentiating Eq. (4) and integrating by parts we find for this purpose

$$\frac{\partial p}{\partial t} \approx \frac{-\rho_0 U^3}{\mathscr{A}(1-M^2)}\left(1+\frac{\mathscr{A}_0}{\mathscr{A}}\right)\int_{-\infty}^{\infty}\frac{\partial \mathscr{A}_T}{\partial x'}(x'+U[t])\frac{\partial^2 \varphi^*}{\partial x'^2}(x',0,0)\,\mathrm{d}x', \quad \frac{x}{\ell_h}\to-\infty. \tag{5}$$

The pressure p is subsequently determined by evaluation of

$$p = \int_{-\infty}^{t}\frac{\partial p}{\partial t'}\,\mathrm{d}t'. \tag{6}$$

3. Optimally distributed hood windows

3.1. Step function approximation

The optimal characteristics of the hood, necessary to produce a linear rise in pressure over a compression wavefront of thickness ℓ_h/M, are derived in the first instance by considering a train with a 'snub-nose', whose nose length $L\to 0$. Then

$$\frac{\partial \mathscr{A}_T}{\partial x}(x+Ut) \to \mathscr{A}_0\delta(x+Ut), \tag{7}$$

and Eq. (2) reduces to

$$p \approx \frac{\rho_0 U^2}{(1-M^2)}\frac{\mathscr{A}_0}{\mathscr{A}}\left(1+\frac{\mathscr{A}_0}{\mathscr{A}}\right)\frac{\partial \varphi^*}{\partial x'}(-U[t],0,0), \quad \frac{x}{\ell_h}\to-\infty, \tag{8}$$

and the pressure gradient becomes

$$\frac{\partial p}{\partial t} \equiv \frac{-\rho_0 U^3}{(1-M^2)}\frac{\mathscr{A}_0}{\mathscr{A}}\left(1+\frac{\mathscr{A}_0}{\mathscr{A}}\right)\frac{\partial^2 \varphi^*}{\partial x'^2}(-U[t],0,0), \quad \frac{x}{\ell_h}\to-\infty. \tag{9}$$

In Eq. (8) it is evident from properties (3) that $\partial\varphi^*/\partial x'$ increases from 0 to 1 as the retarded time increases from a value marginally less than zero to $U[t] > \ell_h$. The hood will therefore behave optimally provided

$$\frac{\partial \varphi^*}{\partial x}(x,0,0) \quad \text{decreases linearly over } -\ell_h < x < 0.$$

Such a variation is described by the straight line

$$\frac{\partial\varphi^*}{\partial x} = v_0 - (1-v_0)\frac{x}{\ell_h}, \quad -\ell_h < x < 0, \tag{10}$$

plotted in Fig. 2, along which $\partial\varphi^*/\partial x$ decreases from 1 at $x = -\ell_h$ to v_0 at the entrance $x = x_0 \equiv 0$ of the hood.

This ideal cannot be realized by a hood having a distribution of discrete windows. If the details of the behaviours of $\partial\varphi^*/\partial x$ near each of the windows are temporarily ignored, the best that can be obtained is a step-like variation of the kind also illustrated in the figure, where $\partial\varphi^*/\partial x$ changes discontinuously at each window. For this simple model, according to which the gross features of $\varphi^*(\mathbf{x})$ in the hood are assumed to depend on x alone, we can set

$$\varphi^* = a_n + \left(v_0 - \frac{(1-v_0)x_n}{\ell_h}\right)x \quad \text{for } x_{n+1} < x < x_n, \ n = 0, \ldots, N, \tag{11}$$

where a_n $(n = 0, 1, \ldots, N)$ are constant coefficients, and where we define $x_{N+1} = -\infty$. Then

$$v_n = v_0 - \frac{(1-v_0)x_n}{\ell_h} \tag{12}$$

is the constant value of $\partial\varphi^*/\partial x$ in the interval $x_{n+1} < x < x_n$ between the windows at $x = x_{n+1}$ and x_n. Therefore, the volume flux q_n, say, through the nth window is just equal to $\mathscr{A}(v_n - v_{n-1})$, or

$$q_n = \frac{\mathscr{A}(1-v_0)}{\ell_h}(x_{n-1} - x_n), \quad n = 1, 2, \ldots, N. \tag{13}$$

The continuity of φ^* at $x = x_n$ requires that the constants a_n satisfy

$$a_n + \left(v_0 - \frac{(1-v_0)x_n}{\ell_h}\right)x_n = a_{n-1} + \left(v_0 - \frac{(1-v_0)x_{n-1}}{\ell_h}\right)x_n, \quad n = 1, \ldots, N, \tag{14}$$

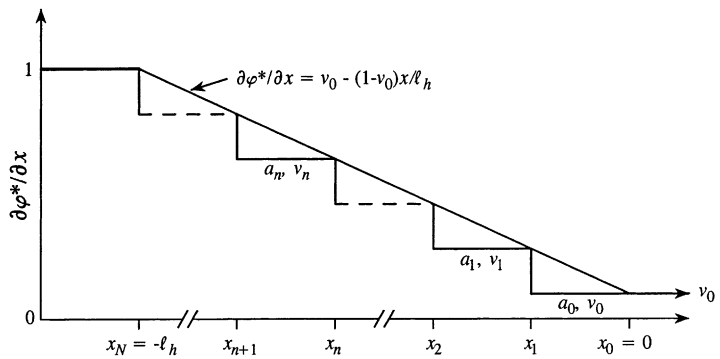

Fig. 2. For an ideal hood,

$$\frac{\partial\varphi^*}{\partial x} = v_0 - (1-v_0)\frac{x}{\ell_h}, \quad -\ell_h < x < 0,$$

represented by the straight line envelope of the step function approximation produced by windows distributed at $x = x_n$, $1 \leqslant n \leqslant N$.

which implies that

$$a_n = a_0 + \frac{(1-v_0)}{\ell_h}\sum_{k=0}^{n} x_k(x_k - x_{k-1}), \quad n = 0, \ldots, N \text{ (taking } x_{-1} = 0). \tag{15}$$

Collecting together these results, the step function approximation becomes

$$\varphi^* = a_0 + \frac{(1-v_0)}{\ell_h}\sum_{k=0}^{n} x_k(x_k - x_{k-1}) + \left(v_0 - \frac{(1-v_0)x_n}{\ell_h}\right)x, \qquad x_{n+1} < x < x_n, \quad n = 0, \ldots, N. \tag{16}$$

3.2. Condition at the hood entrance plane

Formula (16) contains two undefined parameters a_0 and v_0 which are related by conditions to be satisfied at the entrance plane $x = x_0 \equiv 0$ of the hood. To obtain this relation we shall assume that the windows are sufficiently small that the flow at speed v_0 from the hood portal can be approximated locally by the velocity potential for uniform flow from an unflanged circular cylinder. In particular, the first window must therefore be situated at least one or two radii R from the entrance. Then

$$\varphi^* = v_0\varphi_E(\mathbf{x}), \quad x > -R, \tag{17}$$

where

$$\begin{aligned}\varphi_E(\mathbf{x}) &\sim x - \ell'_E \quad \text{as } \frac{x}{R} \to -\infty \text{ inside the hood}\\ &\sim \frac{-\mathscr{A}}{4\pi|\mathbf{x}|} \quad \text{for } |\mathbf{x}| \gg R \text{ outside the hood,}\end{aligned} \tag{18}$$

$\ell'_E \approx 0.61R$ is the end-correction of the hood mouth [16]. It now follows from a comparison of Eqs. (16) and (17) that

$$a_0 = -v_0\ell'_E. \tag{19}$$

3.3. Regularized approximation for φ^*

In order to use these results to obtain a continuous representation of the compression wave pressure distribution (8) it is necessary to modify the step function approximation of $\partial\varphi^*/\partial x$ in the neighbourhoods of the windows. Now $\partial\varphi^*/\partial x$ varies significantly only in the immediate neighbourhood of a window, and assumes the constant value v_n between the $(n+1)$th and nth windows, so that it is actually more convenient to express our formulae in terms of $\partial^2\varphi^*/\partial x^2$ (as in Eq. (9)), which vanishes except near the windows and at the hood portal. To do this we shall assume that on the hood axis the influence of the potential flux q_n from the nth window can be approximated by the incompressible velocity potential

$$\frac{q_n}{\mathscr{A}}\varphi_n(\mathbf{x}),$$

say, produced by a point *sink* of strength q_n at the centroid $(x_n, 0, R)$ of the window.

Introduce cylindrical polar co-ordinates (r,θ,x) defined such that $(z,y)=r(\cos\theta,\sin\theta)$. Then routine calculation [16] yields the formula

$$R\frac{\partial^2\varphi_n}{\partial x^2}(r,\theta,x)=\frac{-1}{\pi}\sum_{m=0}^{\infty}\int_0^{\infty}\frac{\sigma_m\cos(m\theta)\lambda}{\mathrm{I}_{m+1}(\lambda)+\mathrm{I}_{m-1}(\lambda)}\mathrm{I}_m\left(\frac{\lambda r}{R}\right)\cos\left(\frac{\lambda(x-x_n)}{R}\right)\mathrm{d}\lambda,\quad r<R,\tag{20}$$

where I_ν is a modified Bessel function [17], and $\sigma_0=1,\ \sigma_m=2\ (m\geqslant 1)$.

A similar integral expression can be derived [11] for the velocity potential $\varphi_E(\mathbf{x})$ of Eq. (17) describing flow from the hood portal, from which we find

$$\begin{aligned}R\frac{\partial^2\varphi_E}{\partial x^2}(r,\theta,x)&=-\frac{1}{2\pi}\int_0^{\infty}\lambda\mathrm{I}_0\left(\frac{\lambda r}{R}\right)\left(\frac{2\mathrm{K}_1(\lambda)}{\mathrm{I}_1(\lambda)}\right)^{1/2}\cos\left\{\lambda\left(\frac{x}{R}+\mathscr{Z}(\lambda)\right)\right\}\mathrm{d}\lambda,\quad r<R,\\ \mathscr{Z}(\lambda)&=\frac{1}{\pi}\int_0^{\infty}\ln\left(\frac{\mathrm{K}_1(\mu)\mathrm{I}_1(\mu)}{\mathrm{K}_1(\lambda)\mathrm{I}_1(\lambda)}\right)\frac{\mathrm{d}\mu}{\mu^2-\lambda^2},\end{aligned}\tag{21}$$

where K_1 is a modified Bessel function [17].

Hence (taking account of Eq. (17)) the composite representation of $\partial^2\varphi^*/\partial x^2$ for use in Eq. (9) becomes

$$\frac{\partial^2\varphi^*}{\partial x^2}(r,\theta,x)=\sum_{n=1}^{N}\frac{q_n}{\mathscr{A}}\frac{\partial^2\varphi_n}{\partial x^2}(r,\theta,x)+v_0\frac{\partial^2\varphi_E}{\partial x^2}(r,\theta,x),\quad r<R.\tag{22}$$

This is non-zero only within the hood in the vicinities of the windows, and at the hood portal. The monopole strengths q_n are given in terms of v_0 and the window co-ordinates by Eq. (13); the coefficient v_0 remains to be specified.

3.4. Window dimensions

The size of the nth window is estimated by making use of the formula

$$K_n=\frac{q_n}{-\varphi^*(x_n)},\tag{23}$$

where K_n is the Rayleigh *conductivity* of the window [12,15] expressed as the ratio of the volume flux q_n through the window and the total potential rise $-\varphi^*(x_n)$ in the flow direction. Here it is implicitly assumed that the mean value of the potential in the free space region *outside* the hood in the vicinity of the nth window is negligible, in other words, the collective effect of all of the other windows on the exterior potential at the nth window is ignored [13,14].

According to Rayleigh [15], when the area $\mathscr{A}_n$ of the nth window is much smaller than the cross-section $\mathscr{A}$ of the hood and when the hood wall has thickness ℓ_w,

$$\frac{1}{K_n}=\frac{1}{K_n'}+\frac{\ell_w}{\mathscr{A}_n},$$

where $K_n'\approx 2(\mathscr{A}_n/\pi)^{1/2}$ is the conductivity when the wall has zero thickness, i.e.,

$$\frac{1}{K_n}\approx\sqrt{\frac{\pi}{4\mathscr{A}_n}}+\frac{\ell_w}{\mathscr{A}_n}.\tag{24}$$

By solving this equation for $\mathscr{A}_n$ and making use of formulae (13) and (16) to evaluate K_n from Eq. (23), we therefore obtain

$$\mathscr{A}_n \approx \frac{\pi K_n^2}{16}\left(1+\sqrt{1+\frac{16\ell_w}{\pi K_n}}\right)^2,$$
$$K_n = \frac{\mathscr{A}(x_{n-1}-x_n)}{\sum_{k=1}^{n} x_{k-1}(x_k - x_{k-1}) - v_0\ell_h(x_n - \ell'_E)/(1-v_0)}. \tag{25}$$

3.5. Evenly spaced windows

Numerical results are given in Section 4 for the important case in which the windows are evenly spaced along the hood. The step function approximation (16) then assumes the form

$$\varphi^* = -v_0\ell'_E + \frac{n(n+1)(1-v_0)\ell_h}{2N^2} + \left(v_0 + \frac{n(1-v_0)}{N}\right)x, \quad x_{n+1} < x < x_n, \tag{26}$$

where $x_n = -n\ell_h/N$, $0 \leqslant n \leqslant N$, $x_{N+1} = -\infty$. Within the tunnel ($x < x_N = -\ell_h$) $\varphi^* = x - \ell'$, where the end correction

$$\ell' = v_0\ell'_E - \frac{(N+1)(1-v_0)}{2N}\ell_h. \tag{27}$$

The following simplified forms of other formulae given above will also be needed:

$$q_n = \frac{\mathscr{A}(1-v_0)}{N},$$
$$K_n = \frac{2N\mathscr{A}}{n(n-1)\ell_h + 2Nv_0(n\ell_h + N\ell'_E)/(1-v_0)}, \qquad n = 1, \ldots, N, \tag{28}$$

$$\frac{\partial^2\varphi^*}{\partial x^2}(r,\theta,x) = \frac{(1-v_0)}{N}\sum_{n=1}^{N}\frac{\partial^2\varphi_n}{\partial x^2}(r,\theta,x) + v_0\frac{\partial^2\varphi_E}{\partial x^2}(r,\theta,x), \quad r < R. \tag{29}$$

4. Numerical results for evenly spaced windows

4.1. The optimal value of v_0

As x increases from $-\ell_h$ to 0 within an optimally designed hood $\partial\varphi^*/\partial x$ decreases linearly from 1 to v_0. This ideal cannot be attained in a hood with a finite number of windows, but can be closely approximated by choosing the value of v_0 so that the mean value of $R\partial^2\varphi^*/\partial x^2$ is approximately constant. In general, it must be expected that the appropriate value of v_0 will also depend on the position of the train track inside the tunnel. We shall confine attention to the experimental case where the train travels along the tunnel axis ($r = 0$).

For each n and fixed values of r and θ, it is evident from Eq. (20) that $R\partial^2\varphi_n/\partial x^2$ is an even function of $x - x_n$; it exhibits a single maximum negative peak value at $x = x_n$. On the tunnel axis

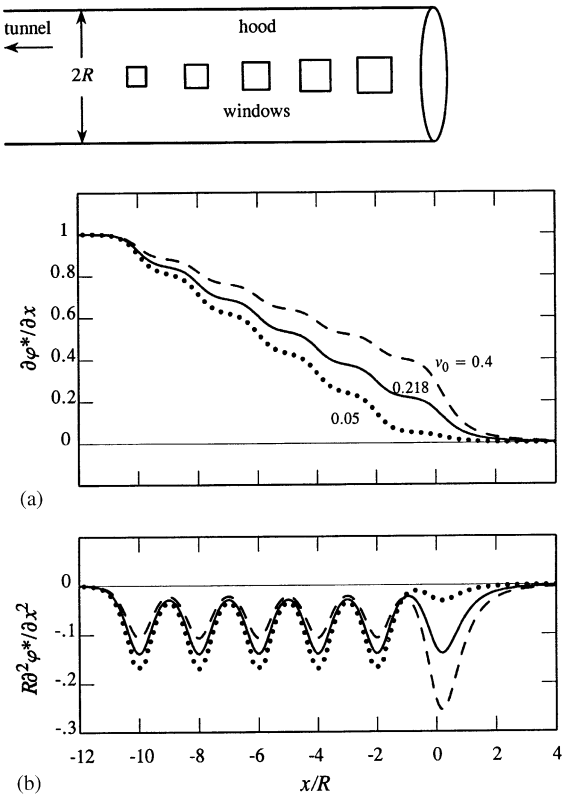

Fig. 3. Calculated variations of (a) $\partial\varphi^*/\partial x$ and (b) $R\partial^2\varphi^*/\partial x^2$ on the hood axis ($r = 0$) for $v_0 = 0.05,\ 0.218,\ 0.4$ in the case of $N = 5$ evenly spaced windows in a hood of length $\ell_h = 10R$. The solid curves are optimal, when v_0 is determined by Eq. (30) and the negative peak values of $R\partial^2\varphi^*/\partial x^2$ are equal.

this maximum value is approximately equal to -0.89. When the windows are evenly spaced the series on the right of Eq. (29) therefore defines a function of x that varies periodically from window to window within the hood, assuming equal negative maxima of $-0.89(1 - v_0)/NR$ at each window, and tending rapidly to zero near the hood portal at $x = 0$. The final term $v_0\partial^2\varphi_E/\partial x^2$ on the right of Eq. (29) is negative and non-zero only near $x = 0$, where it attains a negative maximum value of $-0.64v_0/R$. We can ensure that the *average* negative value of $\partial^2\varphi^*/\partial x^2$ is approximately constant within the hood and in the immediate neighbourhood of the hood portal by requiring all of the peak negative values to be equal, which is the case when

$$v_0 = \frac{1}{1 + 0.72N}. \tag{30}$$

The optimal character of this choice on the hood axis is shown in Fig. 3 for $N = 5$ for a hood of length $\ell_h = 10R$. The solid-line curves in the figure illustrate how $v_0 = 0.218$ determined by Eq. (30) supplies the smoothest variation of $\partial\varphi^*/\partial x$ at the hood portal, and equal negative peak values for $R\partial^2\varphi^*/\partial x^2$ at the windows and at the portal.

4.2. Train with ellipsoidal nose profile

Consider a train with an ellipsoidal nose profile obtained by rotating the curve $y = h\sqrt{(x/L)(2-x/L)}$, $0<x<L$ about the x-axis, so that, when s denotes distance measured from the front of the train (and the tail of the train is at $s=\infty$),

$$\frac{\mathscr{A}_T(s)}{\mathscr{A}_0} = \begin{cases} \dfrac{s}{L}\left(2-\dfrac{s}{L}\right), & 0<s<L, \\ 1, & s>L. \end{cases} \tag{31}$$

This formula has been used to evaluate the compression wave pressure gradient $\partial p/\partial t$ from Eq. (5) for a train entering along the axis of symmetry of a hood of length $\ell_h = 10R$ with evenly spaced and optimally sized windows; $\partial^2\varphi^*/\partial x^2$ is calculated from Eq. (29) when $r=0$ and v_0 is given by Eq. (30). The compression wave pressure profile is then determined from Eq. (6).

Numerical results are given for

$$\frac{\mathscr{A}_0}{\mathscr{A}} = 0.2, \quad \frac{h}{L} = \frac{1}{3}. \tag{32}$$

Fig. 4 depicts the calculated variations of

$$p\Big/\frac{\rho_0 U^2}{(1-M^2)}\frac{\mathscr{A}_0}{\mathscr{A}}\left(1+\frac{\mathscr{A}_0}{\mathscr{A}}\right), \quad \frac{\partial p}{\partial t}\Big/\frac{\rho_0 U^3}{R(1-M^2)}\frac{\mathscr{A}_0}{\mathscr{A}}\left(1+\frac{\mathscr{A}_0}{\mathscr{A}}\right) \tag{33}$$

plotted as functions of $U[t]/R$ for $N=5$ windows (where $[t] = t + (x-\ell')/c_0$, $\ell' \approx -4.6R$). The pressure gradient exhibits six equal maxima, that near $U[t]/R = 0$ being the contribution from $\partial^2\varphi_E^*/\partial x^2$ produced as the nose enters the hood. These maxima in $\partial p/\partial t$ are manifested also by a corresponding 'rippling' of the pressure profile p, which otherwise rises smoothly over

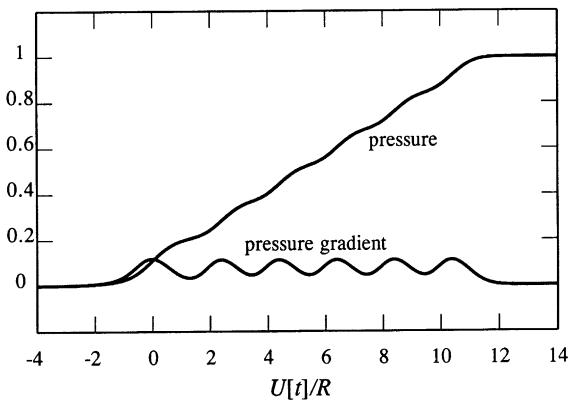

Fig. 4. The normalized compression wave and pressure gradient

$$p\Big/\frac{\rho_0 U^2}{(1-M^2)}\frac{\mathscr{A}_0}{\mathscr{A}}\left(1+\frac{\mathscr{A}_0}{\mathscr{A}}\right), \quad \frac{\partial p}{\partial t}\Big/\frac{\rho_0 U^3}{R(1-M^2)}\frac{\mathscr{A}_0}{\mathscr{A}}\left(1+\frac{\mathscr{A}_0}{\mathscr{A}}\right)$$

produced by a train with the ellipsoidal nose (31) satisfying Eq. (32) entering an optimized hood of length $\ell_h = 10R$ with $N=5$ evenly spaced windows.

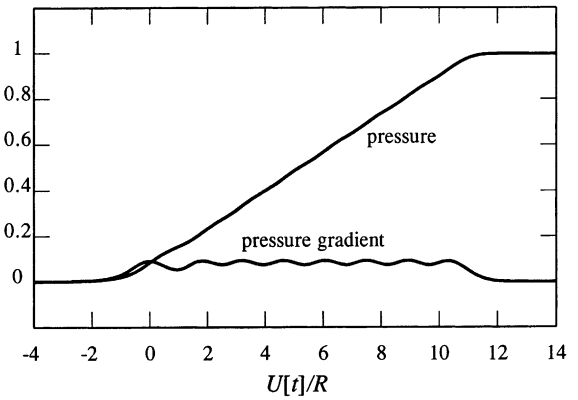

Fig. 5. The normalized compression wave and pressure gradient

$$p\Big/\frac{\rho_0 U^2}{(1-M^2)}\frac{\mathscr{A}_0}{\mathscr{A}}\left(1+\frac{\mathscr{A}_0}{\mathscr{A}}\right),\quad \frac{\partial p}{\partial t}\Big/\frac{\rho_0 U^3}{R(1-M^2)}\frac{\mathscr{A}_0}{\mathscr{A}}\left(1+\frac{\mathscr{A}_0}{\mathscr{A}}\right)$$

produced by a train with the ellipsoidal nose (31) satisfying Eq. (32) entering an optimized hood of length $\ell_h = 10R$ with $N = 7$ evenly spaced windows.

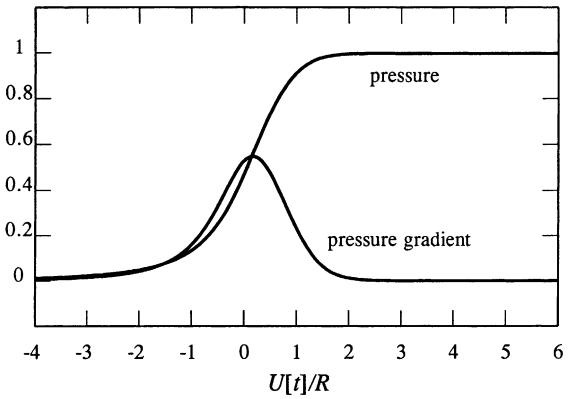

Fig. 6. The normalized compression wave and pressure gradient

$$p\Big/\frac{\rho_0 U^2}{(1-M^2)}\frac{\mathscr{A}_0}{\mathscr{A}}\left(1+\frac{\mathscr{A}_0}{\mathscr{A}}\right),\quad \frac{\partial p}{\partial t}\Big/\frac{\rho_0 U^3}{R(1-M^2)}\frac{\mathscr{A}_0}{\mathscr{A}}\left(1+\frac{\mathscr{A}_0}{\mathscr{A}}\right)$$

produced by a train with the ellipsoidal nose (31) satisfying Eq. (32) entering an unflanged tunnel portal with no hood.

$-1 < U[t]/R < 11$, so that the overall compression wave thickness $\sim 12R/M \gg \ell_h$. A considerable smoothing of the pressure rise is evident in the case illustrated in Fig. 5, where the number of windows is increased to $N = 7$ ($\ell' \approx -4.7R$).

When there are no windows (Fig. 6) the pressure rise occurs over $-1 < U[t]/R < 1$, and the compression wave thickness $\sim 2R/M$. The peak pressure gradient then assumes its the maximum possible value, which is, respectively, about 4.5 and 6.1 times larger than those in Figs. 4 and 5 for $N = 5$ and 7 windows.

Table 1
Square window sides for $N = 5$

ℓ_w/R	ℓ_1/R	ℓ_2/R	ℓ_3/R	ℓ_4/R	ℓ_5/R
0	0.77	0.33	0.18	0.12	0.08
0.15	0.91	0.45	0.29	0.21	0.16
0.30	1.02	0.54	0.36	0.26	0.21

Table 2
Square window sides for $N = 7$

ℓ_w/R	ℓ_1/R	ℓ_2/R	ℓ_3/R	ℓ_4/R	ℓ_5/R	ℓ_6/R	ℓ_7/R
0	0.98	0.45	0.25	0.16	0.11	0.08	0.06
0.15	1.13	0.58	0.37	0.26	0.20	0.16	0.14
0.30	1.25	0.67	0.44	0.33	0.26	0.21	0.18

4.3. The optimal window dimensions

The areas of the optimally sized windows decrease with distance from the hood portal. When $N = 5$ the window centroids are at $x/R = -2, -4, -6, -8, -10$, and the area of the nth window is calculated from the first of Eq. (25) with the conductivity K_n given by Eq. (28). For square windows of side $\ell_n = \sqrt{\mathscr{A}_n}$ the values of ℓ_1 to ℓ_5 are listed in Table 1 for three values of the hood wall thickness $\ell_w = 0,\ 0.15R,\ 0.3R$. The windows increase in size with wall thickness, and the case $\ell_w = 0.15R$ is probably representative of conditions in practice. However, the predicted sizes of the smaller windows may be too small because of the assumption (implicit in our neglect of vortex sources) that the motion in each window is irrotational. Separated flow from the window edges produced by the entering train can generate non-negligible vortex sources that have not been considered in optimizing the window dimensions; such sources tend to block flow through smaller windows which would therefore need to be larger in order to behave optimally.

The tabulated values (and other values calculated from Eqs. (25) and (28) for other values of N) are really only a guide to the actual dimensions. The latter should be determined experimentally, using a model hood fitted with windows whose areas can be varied by means of sliding panels. The experiment starts with the windows set to their theoretically predicted sizes, which are then adjusted to yield optimal performance; adjustments will probably be necessary only for the smaller windows.

A similar cautionary note is necessary when interpreting the sizes given in Table 2 for the other case considered above of $N = 7$ windows.

5. Conclusion

An optimally designed tunnel-entrance hood produces a linear growth in pressure across the wavefront of the compression wave generated by a high-speed train, and a wavefront thickness roughly equal to the ratio of the hood length to the train Mach number. For a hood of uniform

cross-section, with windows along its length, this ideal behaviour is achieved by distributing the window positions and sizes in such a way that the axial velocity $\partial\varphi^*/\partial x$ of a uniform, hypothetical potential flow out of the tunnel and hood decreases linearly to zero over the length of the hood. The function φ^* occurs in the Green's function used to express the compression wave in terms of an equivalent 'source' description of the train. It is only theoretically possible for $\partial\varphi^*/\partial x$ to vary linearly in the hood for a 'continuous' distribution of windows, but our calculations for evenly spaced windows of variable size have shown for a hood of length $\ell_h = 10R$ that as few as seven windows can be expected to produce a compression wavefront pressure profile with minimal 'rippling' and uniformly small pressure gradient (about 17% of that in the absence of windows).

In addition to the source distribution associated with the moving train, vortex dipoles attributable to separation of the air flow over the train, from the hood portal and from the peripheries of the windows, also affect in a small yet significant manner the characteristics of the pressure rise across the compression wavefront. In particular, vorticity generated in the windows can reduce the effective window 'conductivity', and this is not easily quantified without recourse to extensive numerical analysis. This means that our predictions of the optimum window sizes necessary to produce a linear rise in pressure may be too small. Hood design should therefore be finalized using model scale tests to refine predictions obtained by the method of this paper: the theory is first used to predict the window dimensions in the absence of separated flow; the final window sizes are determined from a series of tests that allow predicted optimal window dimensions to be adjusted to take full account of flow separation.

Acknowledgements

The work reported in this paper is sponsored by the Japan Railway Technical Research Institute. The author gratefully acknowledges the benefit of discussions with Dr. Tatsuo Maeda and with Dr. Masanobu Iida.

Appendix. Nomenclature

a_n coefficient in definition (11) of φ^*
A_n area of nth window
$\mathscr{A}$ cross-sectional area of the tunnel
$\mathscr{A}_0$ uniform cross-sectional area of the train
$\mathscr{A}_T$ variable cross-sectional area of the train
c_0 speed of sound
G Green's function
h radius of uniform section of train
H Heaviside step function
K_n Rayleigh conductivity of nth window
ℓ_h length of hood
ℓ_w thickness of tunnel wall
ℓ_x axial length of a window

ℓ_θ azimuthal length of a window
ℓ' end correction
ℓ'_E end correction for circular duct, $\sim 0.61R$
M train Mach number
N total number of windows
p pressure
q_n effective source strength of nth window
U speed of train
R tunnel radius
$[t]$ retarded time
v_0 velocity in expression for φ^*
x_n centroid of the nth window
γ ratio of specific heats
ρ_0 mean air density
φ^* velocity potential in the definition of G
φ_E velocity potential of flow from a circular duct
φ_n velocity potential produced by flow from the nth window

References

[1] T. Hara, Aerodynamic force acting on a high speed train at tunnel entrance, *Quarterly Report of the Railway Technical Research Institute* 2 (2) (1961) 5–11.
[2] T. Hara, M. Kawaguti, G. Fukuchi, A. Yamamoto, Aerodynamics of high-speed train, *Monthly Bulletin of the International Railway Congress Association* XLV (2) (1968) 121–146.
[3] S. Ozawa, Y. Morito, T. Maeda, M. Kinosita, Investigation of the pressure wave radiated from a tunnel exit, Railway Technical Research Institute Report 1023, 1976 (in Japanese).
[4] W.A. Woods, C.W. Pope, Secondary aerodynamic effects in rail tunnels during vehicle entry, *Second BHRA Symposium of the Aerodynamics and Ventilation of Vehicle Tunnels*, Cambridge, England, 23–25 March 1976, Paper C5, pp. 71–86.
[5] S. Ozawa, T. Maeda, Model experiment on reduction of micro-pressure wave radiated from tunnel exit, in: A. Haerter (Ed.), *Proceedings of the International Symposium on Scale Modeling*, Japan Society of Mechanical Engineers, Tokyo, 18–22 July, 1988.
[6] S. Ozawa, T. Maeda, T. Matsumura, K. Uchida, H. Kajiyama, K. Tanemoto, Countermeasures to reduce micro-pressure waves radiating from exits of Shinkansen tunnels, in: *Aerodynamics and Ventilation of Vehicle Tunnels*, Elsevier Science Publishers, Amsterdam, 1991, pp. 253–266.
[7] T. Maeda, T. Matsumura, M. Iida, K. Nakatani, K. Uchida, Effect of shape of train nose on compression wave generated by train entering tunnel, *Proceedings of the International Conference on Speedup Technology for Railway and Maglev Vehicles*, Yokohama, Japan, 22–26 November, 1993, pp. 315–319.
[8] M. Iida, T. Matsumura, K. Nakatani, T. Fukuda, T. Maeda, Optimum nose shape for reducing tunnel sonic boom, Institution of Mechanical Engineers Paper C514/015/96, 1996.
[9] T. Maeda, private communication, 2000.
[10] M.S. Howe, M. Iida, T. Fukuda, T. Maeda, Theoretical and experimental investigation of the compression wave generated by a train entering a tunnel with a flared portal, *Journal of Fluid Mechanics* 425 (2000) 111–132.
[11] M.S. Howe, The compression wave produced by a high-speed train entering a tunnel, *Proceedings of the Royal Society A* 454 (1998) 1523–1534.
[12] M.S. Howe, *Acoustics of Fluid–Structure Interactions*, Cambridge University Press, Cambridge, 1998.

[13] M.S. Howe, The compression wave generated by a high-speed train at a vented tunnel entrance, *Journal of the Acoustical Society of America* 104 (1998) 1158–1164.
[14] M.S. Howe, Prolongation of the rise time of the compression wave generated by a high speed train entering a tunnel, *Proceedings of the Royal Society A* 455 (1999) 863–878.
[15] L. Rayleigh, *The Theory of Sound*, Vol. 2, Macmillan, London, 1926.
[16] B. Noble, *Methods based on the Wiener–Hopf Technique*, Pergamon Press, London, 1958 (reprinted 1988 by Chelsea Publishing Company, New York).
[17] M. Abramowitz, I.A. Stegun (Eds.), *Handbook of Mathematical Functions*, Ninth Corrected Printing, US Department of Commerce, National Bureau of Standards Applied Mathematics Series No. 55, 1970.